Adsorption-Induced Deformation of Microporous Carbons: Pore Size Distribution Effect

Piotr Kowalczyk,*,† Alina Ciach,‡ and Alexander V. Neimark§

Applied Physics, RMIT University, GPO Box 2476V, Victoria 3001, Australia, Institute of Physical Chemistry, Polish Academy of Science, Kasprzaka Street 44/52, 01-224 Warsaw, Poland, and Department of Chemical and Biochemical Engineering, Rutgers, The State University of New Jersey, 98 Brett Road, Piscataway, New Jersey 08854-8058

Received February 5, 2008. Revised Manuscript Received April 10, 2008

We present a thermodynamic model of adsorption-induced deformation of microporous carbons. The model represents the carbon structure as a macroscopically isotropic disordered three-dimensional medium composed of stacks of slit-shaped pores of different sizes embedded in an incompressible amorphous matrix. Adsorption stress in pores is calculated by means of Monte Carlo simulations. The proposed model reproduces qualitatively the experimental nonmonotonic dilatometric deformation curve for argon adsorption on carbide-derived activated carbon at 243 K and pressure up to 1.2 MPa. The elastic deformation (contraction at low pressures and swelling at higher pressures) results from the adsorption stress that depends strongly on the pore size. The pore size distribution determines the shape of the deformation curve, whereas the bulk modulus controls the extent of the sample deformation.

1. Introduction

Understanding the adsorption-induced deformation of microporous solids, in particular carbons, is one of the long-standing problems in adsorption science.[1–5] The phenomenon of adsorption-induced deformation is well documented in the literature.[6–15] The first studies on charcoal swelling were published by Bangham and co-workers[2,3] in 1930, followed by the precise measurements of carbon contraction and expansion performed by Haines and McIntosh.[4] Although mechanical properties of miroporous carbons are critically important for various technological applications,[16–18] the basic mechanisms of deformation during the adsorption−desorption processes are still not completely understood.[1]

Deformation of an adsorbent during adsorption−desorption cycles depends on the internal structure of porous body. It is commonly accepted that the pore structure in activated carbons can be viewed as a disordered array of slit-shaped micropores embedded in an amorphous matrix.[19–26] Due to the presence of micropores, activated carbons possess a large surface area. As a result, the adsorbed molecules produce a significant adsorption stress of the order of GPa.[27–30] This stress may be either positive or negative, depending on the interplay of adsorption and confining effects; it causes either contraction or swelling, respectively.[6,27–31]

There were a few attempts to describe adsorption-induced deformation on the basis of phenomenological thermodynamics.[1,32,33] The most successful approaches to analyzing the experimental data on microporous solids were based on density functional theory and the thermodynamics of vacancy solution.[6,29,33,34] In particular, density functional theory has been instrumental in describing adsorption deformation in ordered microporous materials such as zeolites.[6] In this paper, we extend the thermodynamic approach suggested in ref 6 to adsorption deformation in disordered microporous carbons. However, instead of density functional theory, we employ Monte Carlo simulations

* To whom correspondence should be addressed. Phone: +61 (03) 99252571. Fax: +61 (03) 99255290. E-mail: E72231@ems.rmit.edu.au.
† RMIT University.
‡ Polish Academy of Science.
§ Rutgers, The State University of New Jersey.

(1) Tvardovskiy, A. V. *Sorbent deformation*; Elsevier Ltd.: Oxford, 2007.
(2) Bangham, D. H.; Fakhoury, N. *Nature (London)* **1928**, *122*, 681.
(3) Bangham, D. H. *Trans. Faraday Soc.* **1937**, *33*, 805.
(4) Haines, R. S.; McIntosh, R. *J. Chem. Phys.* **1947**, *15*, 28–38.
(5) Maggs, F. A. P. *Trans. Faraday Soc.* **1946**, *42*, 284.
(6) Ravikovitch, P. I.; Neimark, A. V. *Langmuir* **2006**, *22*, 10864.
(7) Bering, B. P.; Krasilnikova, O. K.; Serpinskii, V. V. *Dokl. Akad. Nauk USSR* **1976**, *231*, 373.
(8) Ivanova, T. N.; Serpinskii, V. V.; Baranova, V. P.; Dubinin, M. M.; Davletshin, R. A. *Bull. Acad. Sci. USSR Div. Chem. Sci.* **1986**, *2*, 273.
(9) Tvardovskiy, A. V.; Fomkin, A. A.; Tarasevich, Yu.I.; Zhukova, A. I. *J. Colloid Interface Sci.* **1999**, *212*, 246.
(10) Yakovlev, V.Yu.; Fomkin, A. A.; Tvardovskiy, A. V. *J. Colloid Interface Sci.* **2003**, *268*, 33.
(11) Fomkin, A. A. *Adsorption* **2005**, *11*, 425.
(12) Scherer, G. W. *J. Am. Chem. Soc.* **1986**, *69*, 473.
(13) Bering, B. P.; Krasilnikova, O. K.; Sarakhov, A. I.; Serpinskii, V. V.; Dubinin, M. M. *Bull. Acad. Sci. USSR Div. Chem. Sci.* **1977**, *26*, 2258.
(14) Fomkin, A. A.; Pulin, A. L.; Izvestiya, A. N. *Bull. Acad. Sci. USSR Div. Chem. Sci.* **1999**, *10*, 1887.
(15) Tvardovskiy, A. V.; Fomkin, A. A.; Tarasevich, Yu.I.; Polyakova, I. G.; Serpinskii, V. V.; Guseva, I. M. *J. Colloid Interface Sci.* **1994**, *164*, 114.
(16) Bansal, R. Ch.; Goyal, M. *Activated Carbon Adsorption*; CRC Press: Boca Raton, FL, 2005.
(17) Marsh, H.; Rodriguez-Reinoso, F. *Activated Carbon*; Elsevier Ltd.: Oxford, 2006.
(18) Gregg, S. J., Sing, K. S. W. *Adsorption, Surface Area and Porosity*: Academic Press: London, 1982.
(19) Nemirovsky, D.; Moreh, R.; Kaneko, K.; Ohba, T.; Mayers, J. *Sur. Sci.* **2003**, *526*, 282.
(20) Nemirovsky, D.; Moreh, R.; Andersen, K. H.; Mayers, J. *J. Phys. Con. Matt.* **1999**, *11*, 6653.
(21) Kaneko, K.; Ishii, C.; Ruike, M.; Kuwabara, H. *Carbon* **1992**, *30*, 1075.
(22) Nguyen, C.; Do, D. D. *Langmuir* **1999**, *15*, 3608.
(23) Heuchel, M.; Jaroniec, M. *Langmuir* **1995**, *11*, 4532.
(24) Muller, E. A.; Hung, F. R.; Gubbins, K. E. *Langmuir* **2000**, *16*, 5418.
(25) Murray, K. L.; Seaton, N. A.; Day, M. A. *Langmuir* **1998**, *14*, 4953.
(26) Heuchel, M.; Davies, G. M.; Buss, E.; Seaton, N. A. *Langmuir* **1999**, *15*, 8695.
(27) Striolo, A.; Chialvo, A. A.; Cummings, P. T.; Gubbins, K. E. *Langmuir* **2003**, *19*, 8583.
(28) Sizov, V. V.; Piotrovskaya, E. M.; Brodskaya, E. N. *Colloid J.* **2003**, *65*, 772.
(29) Ustinov, E. A.; Do, D. D. *Carbon* **2006**, *44*, 2652.
(30) Balbuena, P. B.; Berry, D.; Gubbins, K. E. *J. Phys. Chem.* **1993**, *97*, 937.
(31) Israelachvili, J. N. *Intermolecular and Surface Forces*; Academic Press: London, 1991.
(32) Pan, Z.; Connell, L. D. *Int. J. Coal Geol.* **2007**, *69*, 243.
(33) Jakubov, T. S. *Phys. Chem. Chem. Phys.* **2002**, *4*, 5678.
(34) Rusanov, A. I.; Kuni, F. M. *Russ. J. Gen. Chem.* **2007**, *77*, 371.
(35) Yakovlev, V.Yu.; Fomkin, A. A.; Tvardovskiy, A. V.; Sinitsyn, V. A.; Pulin, A. L. *Russ. Chem. Bull.* **2003**, *52*, 354.

10.1021/la800406c CCC: $40.75
Published on Web 06/04/2008

to compute the adsorption stress. The pore structure heterogeneity is accounted for with a pore size distribution function. The proposed approach is applied to explain deformation of an activated carbon sample upon argon adsorption at 243 K studied in ref 35. The simulation results reproduce a characteristic nonmonotonic behavior of the dilatometric deformation curve with initial contraction followed by swelling. The predicted bulk modulus of about 7 GPa is typical for vitreous carbons[36] and polycrystalline graphite.[50,51]

2. Thermodynamic Methodology

2.1. Theory of the Elastic Stress in Microporous Carbons: Pore Level. Let us first consider a single slit-shaped pore of width H between two graphite planar walls stabilized by some internal elastic elements presented as a virtual spring in figure 1. This model was considered in recent papers.[29,34] The stiffness of the internal elastic elements is characterized by an effective elastic modulus k_H, which may depend on the pore width. During adsorption, the elastic elements can be either stretched or compressed causing an incremental change of the pore width, ΔH.

The linear strain, $\Delta H/H$, and the total external stress, $\sigma(H,p)$, which depends on the adsorbate pressure p, are related by the Hook law

$$\sigma(H,p) = k_H(H)\frac{\Delta H}{H} \tag{1}$$

At the thermodynamic equilibrium, the total stress is given by

$$\sigma(H,p) = \sigma_s(H,p) - p \tag{2}$$

where the adsorption stress $\sigma_s(H,p)$ can be expressed as,[30,37–40]

$$\sigma_s(H,p) = -\left.\frac{\partial \Omega_p}{\partial H}\right|_{T,p} \tag{3}$$

In the above equation, $\Omega_p(H,p)$ denotes the grand thermodynamic potential per unit surface area. The stress eq 2 is referred to as the solvation, or disjoining pressure.[30]

The incremental expansion/contraction of the pore width is given by

$$\Delta H = \frac{1}{k_H(H)}[\sigma_s(H,p) - p]H \tag{4}$$

The pore deformation is directly proportional to the solvation pressure. The elastic modulus scales the extent of the pore deformation. Note that at a given adsorbate pressure p the solvation pressure depends on the pore width H and, as shown below, may be either contracting or stretching. This effect may cause a highly inhomogeneous distribution of the elastic strain on the pore level in the samples with polydispersed pore size distributions. Accounting for this effect is one of the main aims of our work.

2.2. Theory of the Elastic Stress in Microporous Carbons: Sample Level. Represent the carbon sample as a macroscopically isotropic disordered three-dimensional medium composed of stacks of slit-shaped pores of various sizes embedded in an amorphous matrix. We assume that the matrix is incompressible and it transfers the adsorption stress isotropically (like the pressure in liquid). Upon these restrictions, the adsorption-induced deformation is associated with the changes of the pore volumes of individual pores under the action of adsorption stress (solvation/disjoining pressure). The structural heterogeneity is characterized by the pore size distribution function.

Let $S(H)\,dH$ be the surface area of pores of width $(H,H+dH)$. Then, their volume is

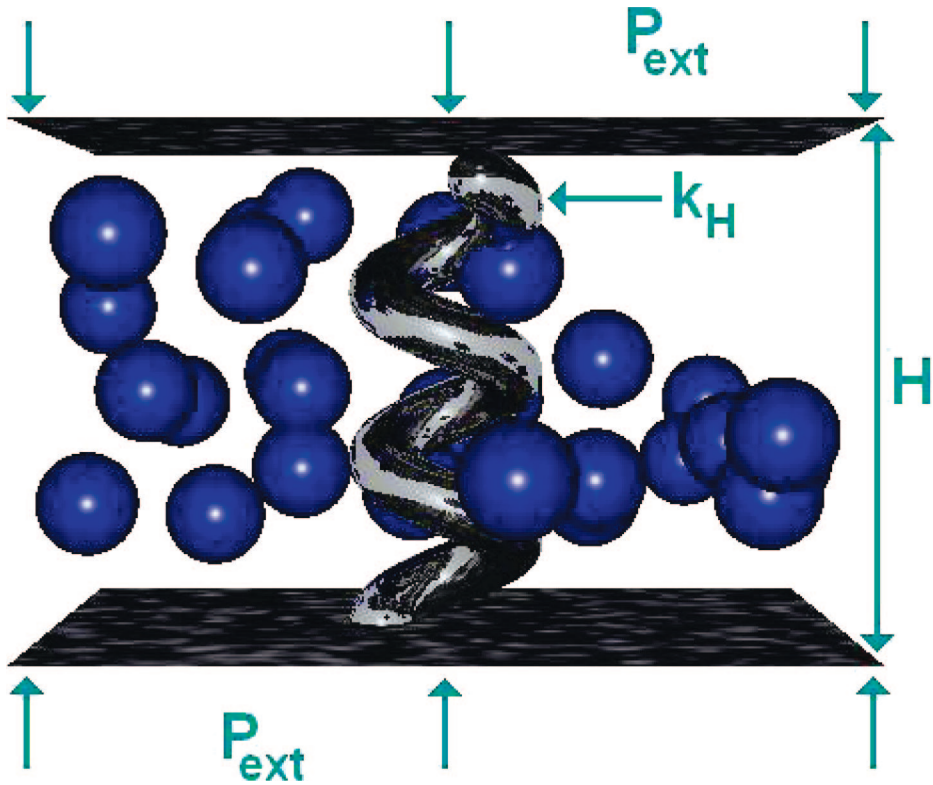

Figure 1. Slit-shaped carbon pore with adsorbed argon molecules: H, pore width; P_{ext}, external pressure; k_H, elastic element characterized by local elastic modulus.

$$V(H)\,\mathrm{d}H = \frac{1}{2}HS(H)\,\mathrm{d}H \tag{5}$$

where $1/2HS(H)\,\mathrm{d}H$ denotes the differential pore size distribution that is commonly calculated from the adsorption isotherms. The cumulative change of the pore volume is given by the following expression,

$$\varepsilon_p = \frac{\Delta V_p}{V_p} = \frac{\int \frac{1}{k_H} H[\sigma_s(H,p) - p]S(H)\,\mathrm{d}H}{\int HS(H)\,\mathrm{d}H} \tag{6}$$

Equation 6 can be simplified further assuming that the elastic modulus k_H does not depend on the pore size, i.e., $k \equiv k_H(H) = \text{const}$.

$$\varepsilon_p = \frac{\Delta V_p}{V_p} = \frac{1}{k}[\overline{\sigma}_s - p] \tag{7}$$

Here, we introduced an effective adsorption stress

$$\overline{\sigma}_s = \frac{\int H\sigma_s(H,p)S(H)\,\mathrm{d}H}{\int HS(H)\,\mathrm{d}H} \tag{8}$$

The quantity measured in dilatometric experiments is the volumetric strain, ε. To relate the sample volumetric strain and the pore volume deformation, we suppose that the carbon matrix is incompressible, that is

$$\varepsilon = \frac{\Delta V_{sample}}{V_{sample}} = \frac{\Delta V_p}{V_p/\varphi} \tag{9}$$

Here, ϕ denotes porosity. Thus,

$$\varepsilon = \frac{\varphi}{k}[\overline{\sigma}_s - p] \tag{10}$$

This relation implies that in the proposed model, the bulk modulus is given by

$$K = \frac{k}{\varphi} \tag{11}$$

In order to calculate the volumetric strain, one first has to compute the adsorption stress in individual pores and then to average this stress with the pore size distribution function.

2.3. Monte Carlo Simulation of Adsorption Stress. The adsorption stress in an individual pore can be determined from eq 3. This method requires the thermodynamic integration along the simulated isotherm to compute the grand thermodynamic potential, and subsequently, the differentiation of the grand thermodynamic potential with respect to H:

$$\Omega_p(\mu,T) = \Omega_p(\mu_r,T) - \int_{\mu_r}^{\mu} N\,\mathrm{d}\mu \tag{12}$$

$$\sigma_s(H,\mu) = k_B T\frac{\partial N(\mu_r)}{\partial H} + \int_{\mu_r}^{\mu}\frac{\partial N}{\partial H}\,\mathrm{d}\mu \tag{13}$$

Here, $N(H,T,\mu)$ is the number of adsorbed molecules per surface area in the pore of width H at given environmental conditions, chemical potential μ and temperature T.

For the slit-shaped geometry (eq 3) can be reduced to,[30]

$$\sigma_s(H,p) = -\int \rho(z)\frac{\partial V_{sf}(z,H)}{\partial H}\,\mathrm{d}z \tag{14}$$

Here, $\rho(z)$ is the density distribution of the adsorbate, and $V_{sf}(z,H)$ is the solid−fluid potential. An advantage of eq 14 is avoiding the differentiation of isotherms with respect to the pore size; however, the fluid density must be calculated quite accurately. In the current paper we determined adsorption stress from eq 13 by using the grand Canonical Monte Carlo (GCMC) simulation method. For comparison purposes, we implemented eq 14 in the gauge cell Monte Carlo simulation method,[41–43] as presented in Figures 1S and 2S.

3. Simulation Methodology

3.1. Fluid−Fluid Interaction Potential. Simulations were performed for argon adsorption in slit-shaped graphitic pores at 243 K. We modeled the argon−argon interactions via the effective truncated one-center Lennard−Jones potential,[44,45]

$$V_{ff}(r) = 4\varepsilon_{ff}\left[\left(\frac{\sigma_{ff}}{r}\right)^{12} - \left(\frac{\sigma_{ff}}{r}\right)^{6}\right]\Theta(r_{cut} - r) \tag{15}$$

Here, r is the distance between two interacting argon molecules, σ_{ff} denotes Lennard-Jones collision diameter, ε_{ff} is the Lennard−Jones well depth, $r_{cut} = 5\sigma_{ff}$ is the cutoff distance, and Θ denotes the Heaviside function. The Lennard−Jones parameters, $\sigma_{ff} = 3.405$ Å, and $\varepsilon_{ff}/k_B = 119.8$ K, (k_B denotes Boltzmann's constant), were taken from previous studies.[46,47]

3.2. Solid−Fluid Interaction Potential. The total argon−carbon interaction potential is a superposition of potentials exerted by opposing walls

$$V_{sf}(z) = V_s(z) + V_s(H - z) \tag{16}$$

The potential $V_s(z)$ is modeled by the 10-4 potential,[48]

$$V_s(z) = 4\pi\sigma_{sf}^2\varepsilon_{sf}\rho_s\left[\frac{1}{5}\left(\frac{\sigma_{sf}}{z}\right)^{10} - \frac{1}{2}\left(\frac{\sigma_{sf}}{z}\right)^{4}\right] \tag{17}$$

where $\rho_s = 38.2$ nm^{-2} is the surface density of carbon atoms, σ_{sf} and ε_{sf} denote the Lennard−Jones solid−fluid collision diameter and well depth, respectively, and z is the distance of the argon molecule from the plane. The parameters of the solid−fluid potential were calculated from the Lorentz−Berthelot mixing rule.[49] For carbon, we adapted the following parameters: $\sigma_{ss} = 3.4$ Å, and $\varepsilon_{ss}/k_B = 28$ K.[49]

3.3. Simulation Details. The adsorption isotherms were computed by the GCMC[38–40] and the gauge cell method.[41–43] We adopted the standard setup for GCMC simulation of adsorption in slit-shaped pore geometry, i.e., cubic simulation box of size $10\sigma_{ff} \times 10\sigma_{ff} \times H$ with periodic boundary conditions and minimum image convention for computing molecular interactions in the x and y directions. The grand canonical ensemble simulations utilized 2×10^8 configurations; the first 1×10^8 configurations were discarded to guarantee equilibration. Fifty nine adsorption isotherms of argon at 243 K and pressures

(36) Sekine, T. *Carbon* **1993**, *31*, 227.
(37) Gogotsi, Y.; Welz, S.; Ersoy, D. A.; McNallan, M. J. *Nature* **2001**, *411*, 283.
(38) Lane, J. E.; Spurling, T. H. *Chem. Phys. Lett.* **1979**, *67*, 107.
(39) Snook, I. K.; van Megen, W. *J. Chem. Phys.* **1980**, *72*, 2907.
(40) Evans, R.; Bettolo Marconi, U. M. *J. Chem. Phys.* **1987**, *86*, 7138.
(41) Neimark, A. V.; Vishnyakov, A. *Phys. Rev. E* **2000**, *62*, 538.
(42) Neimark, A. V.; Ravikovitch, P. I. *Phys. Rev. E* **2002**, *61*, 031505.
(43) Neimark, A. V.; Vishnyakov, A. *J. Chem. Phys.* **2005**, *122*, 234108.
(44) Lee, L. L. *Molecular thermodynamics of nonideal fluids*; Butterworth Publishers: Boston, 1988.
(45) Nose, S. *Mol. Phys.* **1984**, *52*, 255.
(46) Verlet, L. *Phys. Rev.* **1967**, *159*, 98.
(47) Rapaport, D. C. *The art of molecular dynamics simulation*; Cambridge University Press: Cambridge, 1995.
(48) Steele, W. A. *The Interaction of Gases with Solid Surfaces*; Pergamon Press: Oxford, 1974.
(49) Do, D. D. *Adsorption Analysis: Equilibria and Kinetics*; Imperial College Press: London, 1998.
(50) Kelly, B. T. *Physics of Graphite*; Applied Science Publishers: London, 1981.
(51) Boey, S. Y.; Bacon, D. J. *Carbon* **1986**, *24*, 557.

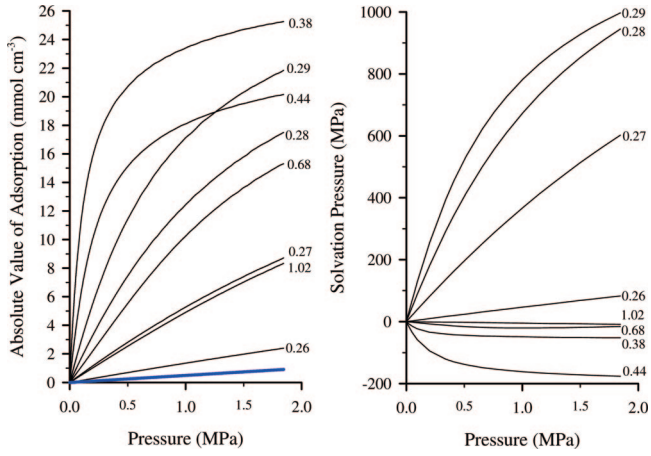

Figure 2. Variation of the absolute value of adsorption (left panel) and solvation pressure (right panel) of argon in a series of slit-shaped carbon pores (an effective pore size, $H_{\text{eff}} = H - 0.34$ nm, is displayed on the plot) at 243 K. The solid blue line on the left panel corresponds to the bulk density of argon at 243 K. Swelling is observed in pores smaller than $\bar{H}_{\text{eff}} = 0.38$ nm, contraction in pores larger than $\bar{H}_{\text{eff}} = 0.38$ nm.

from 1×10^{-4} to 1.86 MPa were computed. All simulated adsorption isotherms of argon consisted of 95 points and covered the range of pore sizes, $H_{\text{eff}} \in [0.23,1.26]$ nm, where $H_{\text{eff}} = H - 0.34$ nm. The thermodynamic integration was performed according to eq 12 with an ideal gas as a reference state.

In the course of the gauge cell MC simulations, the gauge cell volume was adjusted to accumulate ~30 particles. The density profile of adsorbed argon was computed in the pore with the size of the grid $0.1\sigma_{\text{ff}}$. The gauge cell MC utilized 4×10^7configurations, the first 2×10^7 configurations were discarded to guarantee equilibration.

4. Results and Discussions

4.1. Isotherms of Adsorption and Solvation Pressure in Individual Pores. The impact of the pore size on adsorption and solvation pressure is crucial for understanding of the adsorption-induced deformation. As shown earlier,[30,31] the solvation pressure oscillates as a function of the pore size at subcritical temperatures. Here, we study supercritical adsorption at the temperature far exceeding the critical one, and one might expect that the thermal fluctuations should smoothen the packing effects. Nevertheless, we have found a characteristic nonmonotonic dependence of the solvation pressure on the pore size in the range of micropores, given in Figures 2, 3, and 1S. In the range of very small nanopores, both the adsorption and the solvation pressure can reach very high values due to efficient compression of adsorbed molecules, as displayed in Figures 2, 3, 1S, 2S, and 3S. For example, at the external pressure of 1.85 MPa, the solvation pressure in 0.29 nm pore is near 1 GPa, whereas the density of adsorbed argon is ~28 larger than the corresponding bulk density. The simulated adsorption isotherms exhibit type I behavior.[18] In pores larger than 0.38 nm the solvation pressure is negative, as displayed in Figures 2, 3, and 1S. The nonmonotonic character of the dependence of solvation pressure on the pore size is a purely geometrical effect of the molecular packing between smooth walls. When the pore width is $n\sigma_{\text{ff}} < H < (n + 1)\sigma_{\text{ff}}$, here n denotes an integer number, the adsorbed argon cannot form $n + 1$ dense layers, and thus the molecules are packed better in the bulk phase than in the pore. In this case, the solvation pressure is reduced. In contrast, the high compression of molecules in 'perfect' pores of $H = n\sigma_{\text{ff}}$ leads to the increase of the solvation pressure. Due to the high temperature ($T = 243$ K), the pore size

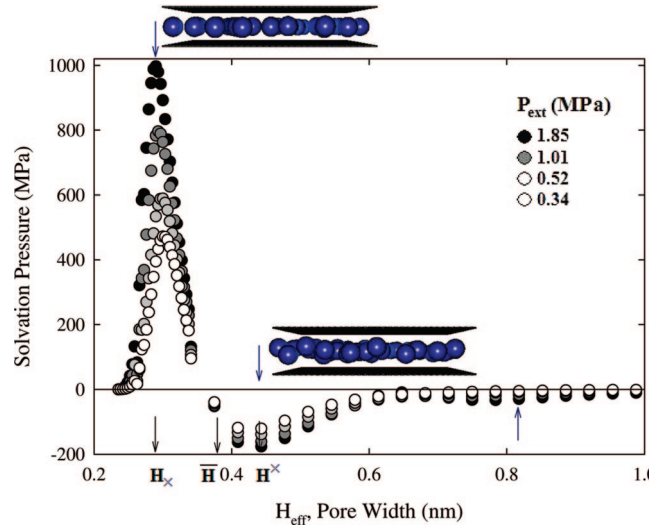

Figure 3. Solvation pressures of argon at 243 K vs slit-shaped carbon pore size. The corresponding external bulk pressures are: 1.85, 1.01, 0.52, and 0.34 MPa. The solvation pressure is positive in swelling pores smaller than $\bar{H} = 0.38$ nm and it is negative in contracting pores ($> \bar{H}$). Maximum solvation pressure is achieved in pores of width $\bar{H}_\times = 0.29$ nm, minimum in pores of width $\bar{H}^\times = 0.44$ nm.

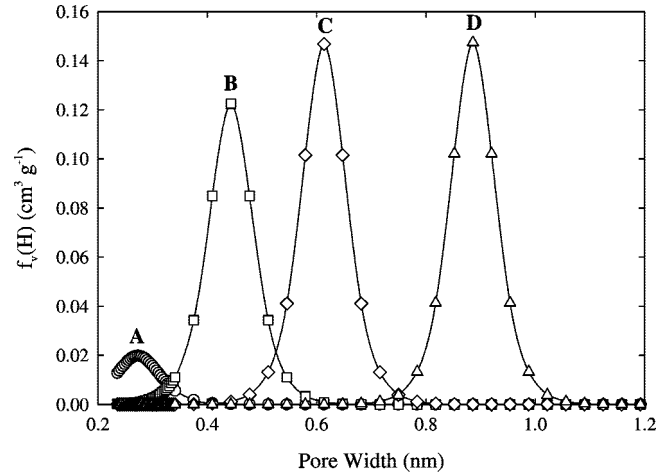

Figure 4. Theoretical pore volume distributions used for the investigation of adsorption-induced deformation of activated carbon upon the argon adsorption at 243 K. For all considered synthetic samples of activated carbons, we assumed the total pore volume 0.47 cm^3/g.

dependence of the solvation pressure is rapidly damped, as shown in Figure 3. Compression of the supercritical argon in pores of $H_{\text{eff}} > 0.8$ nm at considered external conditions is negligible. The accuracy of the thermodynamic integration was confirmed by the series of gauge cell MC simulations, as displayed in Figures 1S and 2S. The densities and the solvation pressures computed from both simulation methods are practically the same that fully validate our computations.

4.2. Analysis of Adsorption-Induced Deformation in Porous Carbon. The pore volume distribution was modeled by the Gaussian functions, as displayed in Figure 4. The corresponding deformation curves and the excess/absolute adsorption isotherms of argon at 243 K are shown in Figures 5 and 6, respectively. It is clearly seen that the internal pore structure greatly impact the deformation curves, while the shape of the nonmonotonic deformation curve is governed by the presence of the pores of different sizes. The nonmonotonic variation of the solvation pressure in the pores of different sizes (see Figures 2 and 3) is reflected in the different shapes of deformation curves for model

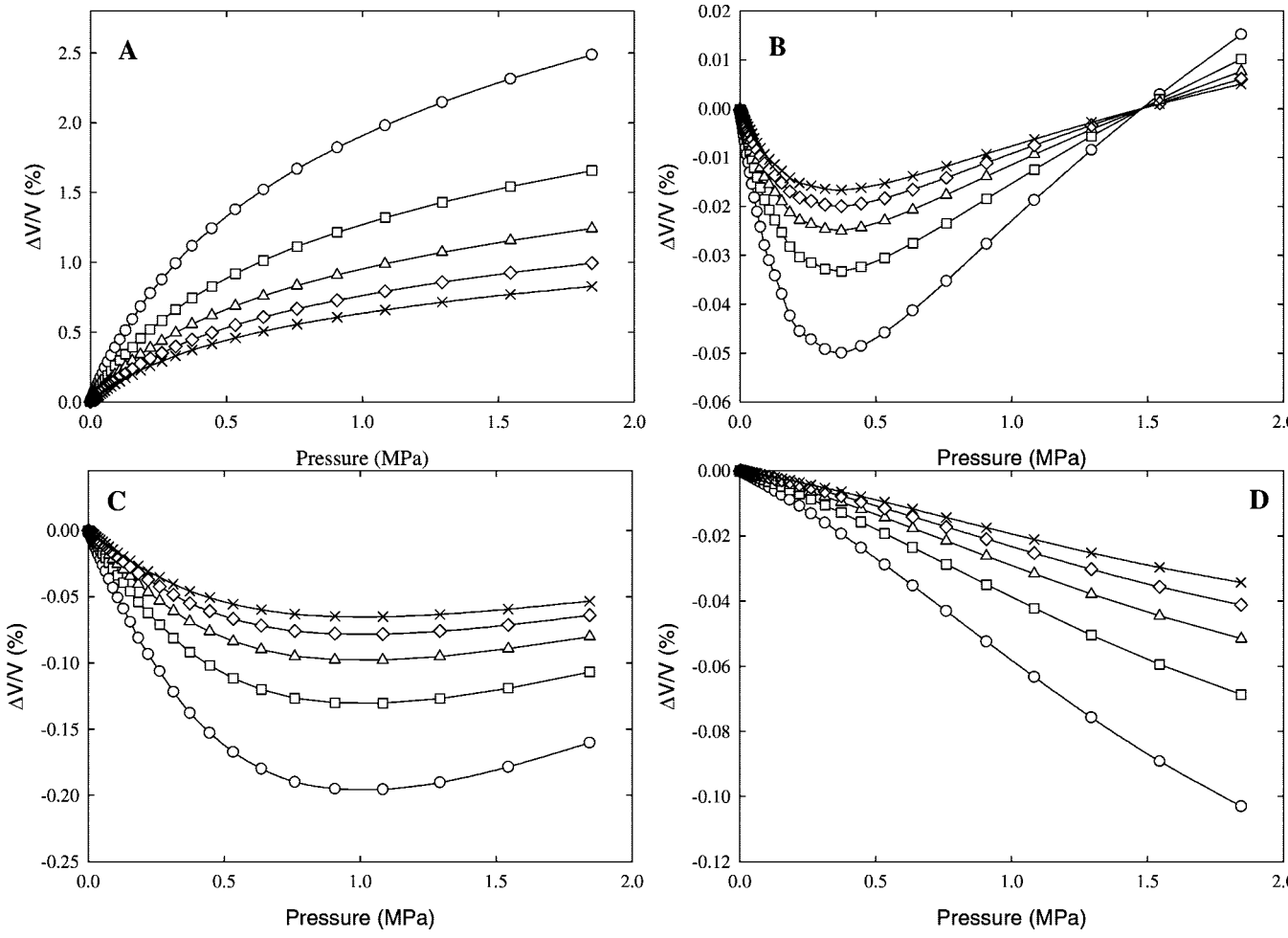

Figure 5. Adsorption-induced deformation curves of argon at 243 K computed on the basis of pore volume distributions displayed in Figure 4. The assumed bulk modulus K is 20 (circles), 30 (squares), 40 (triangles), 50 (diamonds), and 60 (crosses) GPa.

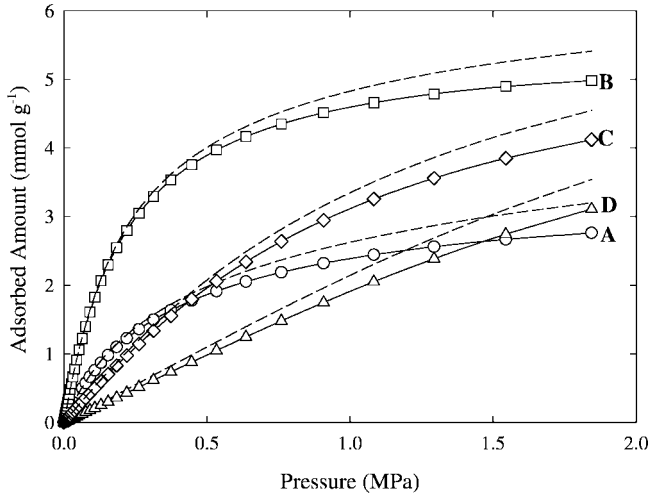

Figure 6. Excess (solid lines) and absolute value (dashed lines) of argon adsorption at 243 K computed on the basis of assumed pore volume distributions displayed in the Figure 4. All isotherms do not depend on the bulk modulus in the considered range $K \in [20,60]$ GPa.

samples A, B, C, and D (see Figure 4). These deformation curves are presented in Figure 5. For the sample A, we observe expansion in the whole range of the pressures. Sample swelling results from the positive solvation pressure in pores of about 0.3 nm. The great excess of the pore pressure compared to the external pressure causes the material to swell and the bulk modulus controls the extent of expansion. Shifting the pore size distribution to the range of wider pores about 0.4 nm leads to nonmonotonic shape of deformation curve (see panel B in figure 5) with initial contraction and further swelling that is typical for data obtained by the dilatometric method.[1] This nonmonotonic shape of the deformation curve is characteristic for many carbons, which contain 'perfect' and 'imperfect' pores. The 'perfect' pores tend to swell due to the positive solvation pressure. In other words, the stress is reduced by the pore expansion. In contrast, 'imperfect' pores tend to contract due to the negative solvation pressure. The experimental deformation curve is a superposition of these two opposite effects. A further shift of the pore volume distribution to the wider range of pore sizes results in the complete excluding of the swelling.

4.3. Comparison with Experimental Data. The simulation model was employed to describe the experimental data collected on a carbide-derived activated carbon during argon adsorption at 243 K characterized by the micropore volume $W_0 = 0.47$ cm^3/g, and the characteristic energy of adsorption $E_0 = 30$ kJ/mol.[1,35] The proposed model predicted a nonmonotonic behavior of experimental dilatometric curve (e.g., $\mu L/L = f(p)$), as displayed in Figure 7. The strain is initially zero and becomes negative (i.e., the sample contracts) as adsorption of argon increases up to external pressure $\approx$0.7 MPa. The maximum measured negative strain is around 0.02% at 243 K and external pressure of 0.1 MPa. After the initial contraction, as adsorption progresses further, the sample expands. The predicted bulk modulus of the investigated carbide-derived activated carbon is 7 GPa. This

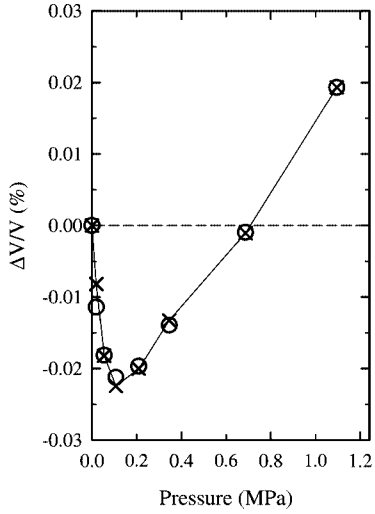

Figure 7. Dependence of the deformation of carbide-derived activated carbon upon the argon adsorption at 243 K measured by the dilatometric method[1,35] (open circles) and computed from the proposed method (crosses).

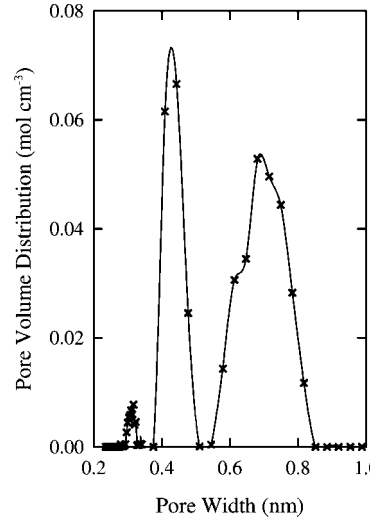

Figure 8. Pore volume distribution of carbide-derived activated carbon computed from experimental deformation-pressure dependence.

value is comparable with the reported data for vitreous carbons[36] and polycrystalline graphite.[50,51] The pore size distribution was determined to provide the best fit with the experimental deformation-pressure dependence. The predicted pore volume distribution is bimodal. The presence of pores of width 0.4−0.8 nm is responsible for the experimentally observed contraction of this material at the first stage of the adsorption process. Pores of width 0.25−0.35 nm swell as the pressure increases.

5. Conclusions

We present a thermodynamic model of adsorption-induced deformation in microporous carbons. The key of this model is the representation of the carbon pore structure as a macroscopically isotropic disordered three-dimensional medium composed of stacks of slit-shaped carbon pores of different sizes embedded in an incompressible amorphous matrix. The model reproduces qualitatively the experimental nonmonotonic shape of dilatometric deformation curve of argon on carbide-derived slit-shaped activated carbon at 243 K and pressure up to 1.2 MPa. We show that the shape of the adsorption-induced deformation curve is determined by the micropore size distribution. The smallest pores of width <0.38 nm (i.e., slightly wider than adsorbate molecular diameter of 0.34 nm) swell, whereas the larger pores (>0.38 nm) contract. The predicted bulk modulus of slit-shaped carbide-derived activated carbon of 7 GPa is characteristic for vitreous carbons[36] and polycrystalline graphite.[50,51]

Acknowledgment. The authors acknowledge the use of the computer clusters (Giza and Cyclone) at the University of Queensland. P.K. acknowledges the Royal Melbourne Institute of Technology (Academic Level B, 2008-2010). P.K. thanks Y. Gogotsi, A. Tvardovskiy, A.P. Terzyk, P.A. Gauden, and T. Nguyen for useful correspondence and discussions. A.V.N. acknowledges support from Quantachrome Instruments.

Supporting Information Available: Additional figures. This material is available free of charge via the Internet at http://pubs.acs.org.

LA800406C